Structure of eigenstates and local spectral density of states: A three-orbital schematic shell model

Wen-ge Wang,[1,2] F. M. Izrailev,[1,3,*] G. Casati[1,4]
[1]*International Center for the Study of Dynamical Systems, University of Milan at Como, via Lucini 3, 22100 Como, Italy*
[2]*Department of Physics, Nanjing University, Nanjing 210093, China*
[3]*Budker Institute of Nuclear Physics, 630090 Novosibirsk, Russia*
[4]*Istituto Nazionale di Fisica della Materia, Unità di Milano, and INFN, Via Celoria 16, 20133, Milano, Italy*
(Received 26 August 1997)

The average shape of the spectral local density of states (LDOS) and eigenfunctions (EFs) has been studied numerically for a conservative dynamical model (three-orbital Lipkin-Meshkov-Glick model) that can exhibit strong chaos in the classical limit. Attention is paid to the comparison of the shape of the LDOS with that known for random matrix models, as well as to the shape of the EFs, for different values of the perturbation strength. The classical counterparts of the LDOS has also been studied and found to be in remarkable agreement with the quantum calculations. Finally, by making use of a generalization of Brillouin-Wigner perturbation expansion, the form of the long tails of the LDOS and EFs is given analytically and confirmed numerically. [S1063-651X(97)13012-4]

PACS number(s): 05.45.+b

I. INTRODUCTION

Recently, growing attention has been paid to the structure of the so-called local spectral density of states (LDOS) as applied to both disordered and dynamical systems that exhibit strong chaotic properties (see, for example, [1–6]). This quantity, known in nuclear physics as the ''strength function,'' is of special interest since it gives information about the ''decay'' of a specific unperturbed state into other states due to interaction. In particular, the width of the strength function defines the effective ''lifetime'' of the unperturbed basis state.

Typically, the shape of the LDOS is assumed to be of Lorentzian form (i.e., the ''Breit-Wigner shape''), as can be analytically derived for sufficiently weak coupling. However, in a direct computation of the Ce atom [1], it was found that at relatively large distances from its center the LDOS has an abrupt decay that is extremely fast (even faster than the exponential). This fact, which is quite generic, is due to the finite range of the interaction in the unperturbed energy basis [7–9]. As a result, matrix elements of a Hamiltonian describing a realistic physical system decay very fast away from the principal diagonal, thus leading to an effective bandlike structure.

Such a band structure of Hamiltonian conservative systems can be compared to one known for unitary evolution operators describing one-dimensional dynamical systems under periodic perturbations, such as the paradigmatic kicked rotator model (KRM) [10,11]. Another example is an ensemble of Hermitian band random matrices (BRMs), which is used to describe quasi-one-dimensional disordered models in solid-state physics (see, for example, [12,13] and references therein). The theory of such ''standard'' BRMs is now well developed (see the review [12]); however, it cannot be applied, verbatim, to conservative systems, such as isolated atoms, nuclei, atomic clusters, etc. The reason is that the Hamiltonians of these latter systems expressed in the basis of the reordered unperturbed states have an additional leading diagonal corresponding to the energy density of the unperturbed Hamiltonian. Band random matrices with such an additional leading diagonal are known as Wigner band random matrices (WBRMs) (see [4,8,14–17]). Unlike the standard BRMs, the theory of WBRMs is not well developed. On the other hand, these matrices are currently under close investigation, since they are believed to provide an adequate description for complex systems (atoms, nuclei, clusters, etc.), as well as for dynamical conservative systems with few degrees of freedom, which are chaotic in the classical limit.

In this paper we consider a specific dynamical model of this type, namely, the so-called Lipkin-Meshkov-Glick model [18]. In our study we follow the approach developed in [4] where the structure of the LDOS and eigenfunctions (EFs) has been numerically investigated in detail for the WBRMs. The main result of [4], which stems from a direct comparison of the LDOS and EFs, is the discovery of the so-called ''localization in the energy shell'' for conservative systems with chaotic behavior. It is of great interest to apply the approach suggested in [4] to dynamical systems of interacting particles.

In this connection it may be interesting to remark that it is possible to relate specific properties of chaotic eigenstates to such observables as the occupation numbers for single-particle levels and transition amplitudes (see details in [19–22]). The above approach [19–22] has been developed for the model of two-body random interaction, by assuming completely random two-body matrix elements. Thus, it is important to extend this approach to dynamical systems of interacting particles with a chaotic dynamics.

The paper has the following structure. In Sec. II we describe the three-orbital Lipkin-Meshkov-Glick (LMG) model and discuss its general properties. The classical limit is con-

*Present address: Instituto de Fisica, Universidad Autonoma de Puebla, Apdo. Postal J-48, Col. San Manuel, Puebla, Puebla, 72570, Mexico. Electronic address: izrailev@physics.spa.umn.edu

sidered in Sec. III, where the transition to chaos that depends on the strength of the perturbation is studied. Section IV is devoted to the discussion of the general properties of eigenstates and spectrum statistics for the quantum model. In Sec. V we numerically investigate the structure of the LDOS and eigenfunctions for different values of model parameters. In Sec. VI, we present some analytical and numerical results for the long tails of the LDOS and eigenfunctions. Concluding remarks are given in Sec. VII.

II. THREE-ORBITAL LMG MODEL

The three-orbital Lipkin-Meshkov-Glick model [18], or for short, the LMG model, is known as some simplification of the shell-model of the nucleus. It was introduced also to check the validity of approximate many-body techniques, including the random-phase approximation and the Bardeen-Cooper-Schrieffer (BCS) theory. The symmetric states of the LMG model, which we will use in our calculations, correspond to collective motions that may mimic the collective motion of the nucleus.

The model has Ω particles distributed among three single-particle orbitals with the same parity and angular momentum. Each orbital is Ω-fold degenerate. The ground, first, and second excited orbitals are labeled by $r=0,1,2$, and the degenerate states within each orbital are labeled by $\gamma=1,2,3,\ldots,\Omega$. The energy of each orbital is denoted by ϵ_r. In our calculations, for simplicity (without the loss of generality), we will set $\epsilon_0=0$.

The Hamiltonian of the model is

$$H=H^0+\lambda V, \tag{1}$$

where

$$H^0=\epsilon_1\left[\sum_{\gamma=1}^{\Omega} a_{1\gamma}^{\dagger}a_{1\gamma}\right]+\epsilon_2\left[\sum_{\gamma=1}^{\Omega} a_{2\gamma}^{\dagger}a_{2\gamma}\right],$$

$$\begin{aligned}V=&\mu_1\left[\sum_{\gamma=1}^{\Omega}\sum_{\gamma'=1}^{\Omega}(a_{1\gamma}^{\dagger}a_{0\gamma}a_{1\gamma'}^{\dagger}a_{0\gamma'}+a_{0\gamma}^{\dagger}a_{1\gamma}a_{0\gamma'}^{\dagger}a_{1\gamma'})\right]\\&+\mu_2\left[\sum_{\gamma=1}^{\Omega}\sum_{\gamma'=1}^{\Omega}(a_{2\gamma}^{\dagger}a_{0\gamma}a_{2\gamma'}^{\dagger}a_{0\gamma'}+a_{0\gamma}^{\dagger}a_{2\gamma}a_{0\gamma'}^{\dagger}a_{2\gamma'})\right]\\&+\mu_3\left[\sum_{\gamma=1}^{\Omega}\sum_{\gamma'=1}^{\Omega}(a_{2\gamma}^{\dagger}a_{1\gamma}a_{2\gamma'}^{\dagger}a_{0\gamma'}+a_{0\gamma}^{\dagger}a_{2\gamma}a_{1\gamma'}^{\dagger}a_{2\gamma'})\right]\\&+\mu_4\left[\sum_{\gamma=1}^{\Omega}\sum_{\gamma'=1}^{\Omega}(a_{1\gamma}^{\dagger}a_{2\gamma}a_{1\gamma'}^{\dagger}a_{0\gamma'}+a_{0\gamma}^{\dagger}a_{1\gamma}a_{2\gamma'}^{\dagger}a_{1\gamma'})\right],\end{aligned} \tag{2}$$

where $a_{r\gamma}^{\dagger}$ and $a_{r\gamma}$ are fermionic creation and annihilation operators obeying the usual anti-commutation relations, and the parameters $\lambda,\mu_1,\mu_2,\mu_3,\mu_4$ describe the strength of the perturbation.

The Hamiltonian (2) can be expressed in a much simpler form. To this end we introduce the two-fermion operators

$$K_{rs}=\sum_{\gamma=1}^{\Omega} a_{r\gamma}^{\dagger}a_{s\gamma}, \quad r,s=0,1,2. \tag{3}$$

The operators K_{00}, K_{11}, and K_{22} are number operators of the orbitals 0, 1, and 2; and K_{rs} for $r\neq s$ are particle raising and lowering operators, respectively. The commutation relations for K_{rs} are

$$[K_{rs},K_{r's'}]=K_{rs'}\delta_{r's}-K_{r's}\delta_{rs'}. \tag{4}$$

As a result, the Hamiltonian can be written as a function of K_{rs},

$$H=H^0+\lambda V, \quad H^0=\epsilon_1K_{11}+\epsilon_2K_{22}, \quad V=\sum_{t=1}^{4}\mu_tV^{(t)}, \tag{5}$$

where

$$\begin{aligned}&V^{(1)}=K_{10}K_{10}+K_{01}K_{01}, \quad V^{(2)}=K_{20}K_{20}+K_{02}K_{02},\\&V^{(3)}=K_{21}K_{20}+K_{02}K_{12}, \quad V^{(4)}=K_{12}K_{10}+K_{01}K_{21}.\end{aligned} \tag{6}$$

The nine operators K_{rs} have a very important property, namely, they are invariant under the interchange of the single-particle-state labels γ. Thus, the Hamiltonian also is invariant under the interchange of γ and conserves the permutation symmetry of the labels γ. This makes it possible to divide the Hilbert space into subspaces according to permutation symmetry. In our quantum calculations, we use a subspace composed of the so-called symmetric states. A convenient basis $|mn\rangle$ for such a subspace can be obtained by operating the symmetric raising operators K_{10} and K_{20} on the state with all the Ω particles in the ground orbital, labeled by $|00\rangle$,

$$|mn\rangle=C(m,n)K_{10}^mK_{20}^n|00\rangle, \tag{7}$$

where $C(m,n)$ is the normalizing coefficient. These states $|mn\rangle$ are eigenstates of the number operators K_{11} and K_{22} with m being the number of particles in the orbital 1 and n the number of particles in the orbital 2. By conservation of particles number, $\Omega=K_{00}+K_{11}+K_{22}$, the population of the ground orbital is $\Omega-m-n$. The dimension of the symmetric subspace is $N=(\Omega+1)(\Omega+2)/2$. Notice that $|00\rangle=a_{0\Omega}^{\dagger}\cdots a_{02}^{\dagger}a_{01}^{\dagger}|00\cdots0\rangle$, and therefore, $|mn\rangle$ are antisymmetric under interchange of label γ.

From Eq. (4) it is seen that the particle raising operators K_{10} and K_{20} commute (as a consequence of their two-fermionic feature), and therefore, the state $|mn\rangle$ in (7) is symmetric under the interchange of the order of raising particles. In this sense, raising fermions from the ground orbital to the two excited orbitals is similar to creation of bosons. Indeed, resorting to the generator coordinate method approach to the dynamic group representation, a boson representation has been found for the symmetric states [23,24]. The above basis states in the boson representation are

$$|mn\rangle=\frac{(b_1^\dagger)^m(b_2^\dagger)^n}{\sqrt{(m+1)!(n+1)!}}|00\rangle \tag{8}$$

where $b_r^\dagger$ are creation operators of bosons. The relations between the operators K_{rs} and the creation and annihilation operators of bosons $b_r^\dagger$ and b_r are

$$K_{rs}=b_r^\dagger b_s$$
$$K_{r0}=K_{0r}^\dagger=b_r^\dagger\sqrt{\Omega-b_1^\dagger b_1-b_2^\dagger b_2}$$
$$[b_r,b_s^\dagger]=\delta_{rs},\quad [b_r,b_s]=[b_r^\dagger,b_s^\dagger]=0 \tag{9}$$

for $r,s=1,2$. Making use of these relations it is easy now to obtain the expressions for the matrix elements of $V^{(t)}$

$$\langle m'n'|K_{10}K_{10}|mn\rangle=\sqrt{(\Omega-m-n)(\Omega-m-n-1)(m+1)(m+2)}\,\delta_{m',m+2}\delta_{n',n},$$
$$\langle m'n'|K_{20}K_{20}|mn\rangle=\sqrt{(\Omega-m-n)(\Omega-m-n-1)(n+1)(n+2)}\,\delta_{m',m}\delta_{n',n+2},$$
$$\langle m'n'|K_{21}K_{20}|mn\rangle=\sqrt{m(\Omega-m-n)(n+1)(n+2)}\,\delta_{m',m-1}\delta_{n',n+2},$$
$$\langle m'n'|K_{12}K_{10}|mn\rangle=\sqrt{n(\Omega-m-n)(m+1)(m+2)}\,\delta_{m',m+2}\delta_{n',n-1}. \tag{10}$$

which can also be found from the commutation relations (4); see [25].

The states $|mn\rangle$ are eigenstates of H^0 with eigenenergies

$$E_{mn}^0=m\epsilon_1+n\epsilon_2. \tag{11}$$

It is convenient to rearrange the eigenstates of H^0 in order of increasing energy, and we will label them by $|\phi_i\rangle$,

$$H^0|\phi_i\rangle=E_i^0|\phi_i\rangle,\quad E_{i+1}^0\geqslant E_i^0. \tag{12}$$

Correspondingly, the eigenstates of the total Hamiltonian H, also reordered in energy, will be labeled by $|\psi_\alpha\rangle$

$$H|\psi_\alpha\rangle=E_\alpha|\psi_\alpha\rangle. \tag{13}$$

In our numerical computations of the LMG model, we take $\Omega=40$; therefore, the dimension of the symmetric subspace is $N=861$. As to the choice of ϵ_1 and ϵ_2, we assume, without loss of generality, $\epsilon_1=1.1$ and $\epsilon_2=1.61$.

The expressions for $V^{(t)}$ in Eqs. (6) and (10) show that each $V^{(t)}$ couples the basis state $|\phi_i\rangle$ with only two other states $|\phi_j\rangle$ with the same energy difference $d^{(t)}=|E_i^0-E_j^0|$, where $d^{(1)}=2\epsilon_1$, $d^{(2)}=2\epsilon_2$, $d^{(3)}=2\epsilon_2-\epsilon_1$, and $d^{(4)}=2\epsilon_1-\epsilon_2$. The average coupling strength $v^2=\langle V_{ij}^2\rangle$ can be found by averaging over the nonzero matrix elements only. Similarly, for each $V^{(t)}$ one can introduce $(v^{(t)})^2=\langle(V_{jk}^{(t)})^2\rangle$, with the average taken over only the nonzero matrix elements of $V^{(t)}$, respectively. Therefore, $\rho^{(t)}\equiv v^{(t)}/d^{(t)}$ is a natural measure of the strength of $V^{(t)}$ with respect to the energy distance between the basis states coupled by $V^{(t)}$. The parameters μ_t in Eq. (5) are determined by the condition that $\rho^{(t)}=1$ for $t=1,2,3,4$, so that, on average, the relative strengths of $V^{(t)}$ are the same. Under this condition, we have $\mu_1\approx0.0116$, $\mu_2\approx0.0169$, $\mu_3\approx0.0158$, and $\mu_4\approx0.00439$, and the estimate of the average coupling strength is $v\approx2.24$.

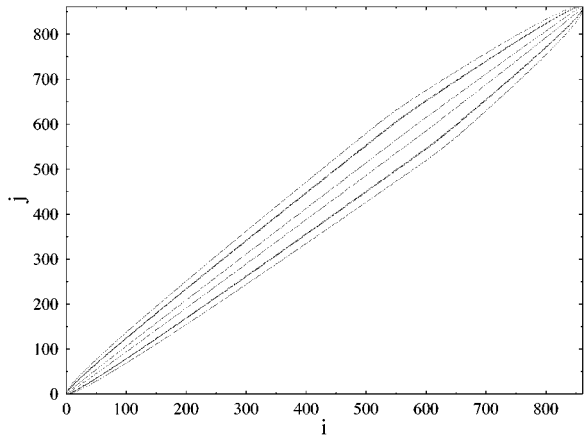

FIG. 1. Global structure of the Hamiltonian matrix. The points represent the nonzero off-diagonal elements $\langle\phi_j|V|\phi_i\rangle$ of the Hamiltonian H.

The global structure of the Hamiltonian matrix is presented in Fig. 1, where points represent nonzero off-diagonal elements $\langle\phi_i|V|\phi_j\rangle$ of the Hamiltonian H. As one can see, the matrix is sparse and bandlike. More precisely, the nonzero elements of the perturbation form only eight curves, since a basis state $|\phi_i\rangle$ is coupled by V to at most eight other basis states. The two inner curves result from the contribution of $V^{(4)}$, while the two outer curves come from $V^{(2)}$. Since $d^{(1)}=2.2\approx d^{(3)}=2.12$, the curves corresponding to $V^{(1)}$ and $V^{(3)}$ are very close to each other and are not separated in the figure. The half-band width b depends on E_i^0 and can be analytically estimated to be $b\approx3E_i^0/\epsilon_2$ for $E_i^0<E'$, and $b\approx2\Omega-6(E_i^0-E')/\epsilon_2$ for $E_i^0>E'$, where $E'\approx2\Omega\epsilon_2/3$. In particular, the maximum width (in the center of the band) is $b_{max}\approx2\Omega$.

The unperturbed density of states $\rho(E^0)$ of H^0 is shown in Fig. 2(a), and turns out to be in agreement with the estimate $\rho(E^0)\approx b/d^{(2)}$. The perturbed density of states $\rho(E)$ is shown in Fig. 2(b) for $\lambda=2.0$. For a better comparison of $\rho(E)$ with $\rho(E^0)$, it is convenient to rescale to the same total energy interval, namely, $\rho(E)\to\rho_\nu(E)=\nu\rho(E\nu)$, where ν is

$$\nu=\frac{(E_{861}-E_1)}{(E_{861}^0-E_1^0)}. \tag{14}$$

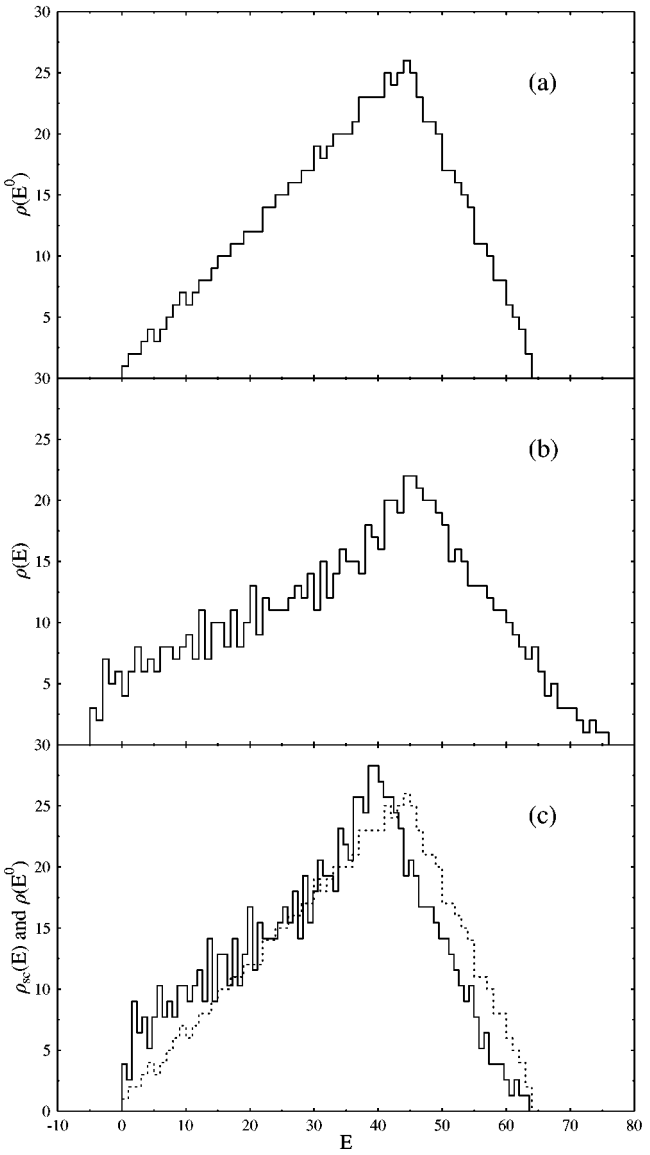

FIG. 2. (a) Unperturbed density of states $\rho(E^0)$ of H^0. (b) Density of states $\rho(E)$ of the system H for $\lambda=2$. (c) The rescaled density of states $\rho_\nu(E)$ for $\lambda=2$ (solid histogram) compared with the unperturbed density of states $\rho(E^0)$ (dashed histogram).

Here, E_{861} and E^0_{861} are the highest eigenenergies of H and H^0, respectively. The ground-state energy of the perturbed Hamiltonian has also been shifted to coincide with the unperturbed one. From the result of such rescaling, shown in Fig. 2(c), one can conclude that the rescaled perturbed density of states is similar to the unperturbed one. For weaker perturbations, $\lambda\leqslant 1$, the correspondence is much better. From Fig. 2(c) one can also see that the peak of $\rho(E)$ is shifted a little towards the center of the spectrum. Moreover, for even stronger perturbations, the peak has been found to be at the center of the spectrum. These properties of the global structure of the Hamiltonian and of the density of states will be used below when we discuss other properties of the model.

III. THE CLASSICAL LIMIT

The classical limit of the symmetric subspace of the LMG model can be obtained by two methods. One method was used in [25] and consists in the direct study of the motion of coherent states in the limit $\Omega\to\infty$. The other method, which will be used here, is based on the boson representation; however, since the boson representation of the symmetric states is obtained via the coherent-state representation, the two methods are basically equivalent.

In order to obtain the classical limit, we introduce the transformation,

$$b_r^\dagger=\sqrt{\frac{\Omega}{2}}(q_r-ip_r),\quad b_r=\sqrt{\frac{\Omega}{2}}(q_r+ip_r),\qquad (15)$$

for $r=1,2$. According to Eqs. (9) and (15), q_r and p_s obey the following commutation rules:

$$[q_r,p_s]=\frac{i}{\Omega}\delta_{rs}.\qquad (16)$$

Therefore, the factor $1/\Omega$ plays the role of Planck constant. Letting the particles number $\Omega\to\infty$, while keeping constant the following parameters

$$\epsilon_1'=\epsilon_1\Omega,\quad \epsilon_2'=\epsilon_2\Omega,\quad \mu_t'=\mu_t\Omega^2,\quad t=1,2,3,4,\qquad (17)$$

one obtains the classical counterpart of the Hamiltonian H,

$$H_{cl}=H^0_{cl}+\lambda V_{cl},\qquad (18)$$

where

$$H^0_{cl}=\frac{\epsilon_1'}{2}(p_1^2+q_1^2)+\frac{\epsilon_2'}{2}(p_2^2+q_2^2),$$

$$V_{cl}=\sum_{t=1}^{4}\mu_t' V_{cl}^{(t)}$$

$$=\mu_1'(q_1^2-p_1^2)(1-G/2)+\mu_2'(q_2^2-p_2^2)(1-G/2)$$

$$+\frac{\mu_3'}{\sqrt{2}}[(q_2^2-p_2^2)q_1+2q_2p_1p_2]\sqrt{1-G/2}$$

$$+\frac{\mu_4'}{\sqrt{2}}[(q_1^2-p_1^2)q_2+2q_1p_1p_2]\sqrt{1-G/2},\qquad (19)$$

with $G=q_1^2+p_1^2+q_2^2+p_2^2=2(b_1^\dagger b_1+b_2^\dagger b_2)/\Omega\leqslant 2$. Notice that the perturbation V_{cl} depends also on momentum variables.

In order to understand the qualitative properties of the classical model, we have plotted the Poincaré surfaces of section at different energies. As in [23,25], it was found that regular regions of phase space are gradually destroyed when λ increases. However, due to the specific form of the classical Hamiltonian H_{cl} in Eq. (19), it has been found that the motion on low- and high-energy surfaces can exhibit more chaotic features than on the medium-energy surfaces. Three typical examples for $\lambda=0.9$ are shown in Fig. 3. The first figure, Fig. 3(a), shows the surface of section at energy $E=10$. It can be seen that trajectories on this energy surface are chaotic, except in a small region. The next, Fig. 3(b), corresponds to the energy $E=39$, in the middle of the energy

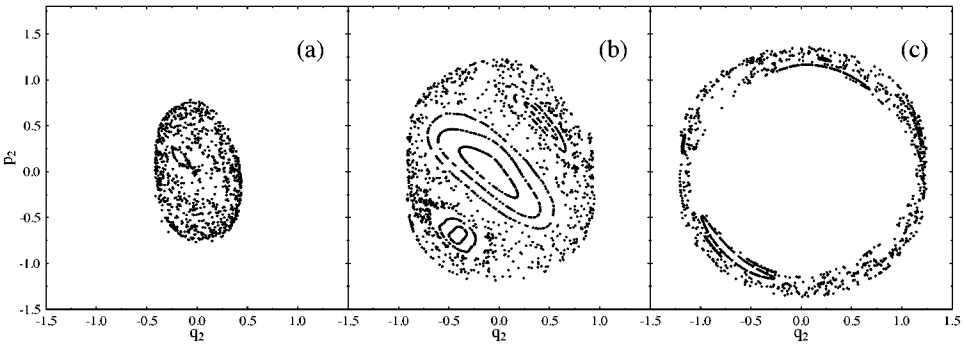

FIG. 3. Poincaré surfaces of section on the (q_2, p_2) plane with $q_1 = 0$ for $\lambda = 0.9$ and (a) $E = 10$, (b) $E = 39$, and (c) $E = 57$.

region. Here one can distinguish three regular islands. Finally, Fig. 3(c) corresponds to the energy $E = 57$ in the high-energy region. Here most trajectories are seen to be chaotic with some remaining regular islands. Note that the central region in Fig. 3(c) is energetically inaccessible. When λ increases to 2.0, it has been found that almost all regular islands disappear and the system is nearly totally chaotic (Fig. 4).

The above peculiar behavior is due to the particular structure of the perturbation V_{cl}. Indeed, at energy $E = 39$, the value of G can be closer to 2 than for the case with $E = 10$. Therefore, due to the terms containing $(1 - G/2)$ in Eq. (19), the perturbation at the energy $E = 10$ is stronger than at $E = 39$. For high energies, instead, since G is quite close to 2, the derivatives $\partial V_{cl}/\partial p_i$ and $\partial V_{cl}/\partial q_i$ can be large and, as a consequence, the motion at high energies ($E = 57$) is more irregular than that at the middle ones.

IV. GENERAL PROPERTIES OF EIGENSTATES AND SPECTRUM STATISTICS

In the preceding section, we have discussed the classical counterpart of the LMG model. In particular, we showed that for not very large perturbations, the classical motion on low- and high-energy surfaces is more irregular than on the middle ones. In this section, we study some general properties of the quantum model, which are related to the above classical features.

In Figs. 5 and 6 we show four typical eigenstates $|\psi_\alpha\rangle$ of the total Hamiltonian H for $\lambda = 0.9$ and $\alpha = 50$–53 and 430–433, respectively, in the basis states $|\phi_i\rangle$ (many-particle states of the unperturbed Hamiltonian H^0). For low levels $\alpha = 50$–53, the states $|\psi_\alpha\rangle$ mainly occupy the region $i = 0$–200 of the basis states $|\phi_i\rangle$, and the expansion coefficients look random in the region. For the levels in the middle of the energy spectrum, $\alpha = 430$–433, the components of the eigenstates $|\psi_\alpha\rangle$ are mainly distributed in the region $i = 200$–700, but the expansion coefficients do not appear as completely random. For example, the coefficients $\langle\phi_i|\psi_\alpha\rangle$ for $\alpha = 433$ seem to be random, without any structure; instead, for $\alpha = 431$, they look sparse and some structure is seen. These figures suggest that eigenstates with low energies are more chaotic in the region $i \in [1,200]$ than those with middle energies in the region $i \in [200,700]$. This is also confirmed by nearest-level-spacing distributions. In Fig. 7 we plot the nearest-level-spacing distributions $P(s)$ for eight different regions in the energy spectrum of H for $\lambda = 0.9$. In order to achieve better statistics we have diagonalized the Hamiltonian with five different values of λ close to $\lambda = 0.9$ and put together the unfolded sequences ΔE_α. As expected, the histograms of $P(s)$ for the lowest- and highest-energy regions are closer to the Wigner-Dyson distribution (dashed lines) than to the Poisson distribution (dashed-dotted lines), while for α in the interval [440,550], $P(s)$ is closer to the Poisson distribution. On the other hand, when λ increases to 2, the level spectrum distribution $P(s)$ becomes very close to the Wigner-Dyson distribution, even in the middle energy region.

The above numerical results are related to properties of the perturbation V, which are determined by the four operators $K_{10}K_{10}$, $K_{20}K_{20}$, $K_{21}K_{20}$, and $K_{12}K_{10}$. So, one needs to study only nonzero matrix elements of these four operators. For example, according to Eq. (10), for a fixed basis state $|\phi_i\rangle$, there is only one basis state $|\phi_j\rangle$ for which the matrix element $\langle\phi_j|K_{10}K_{10}|\phi_i\rangle$ is nonzero. Therefore, the nonzero

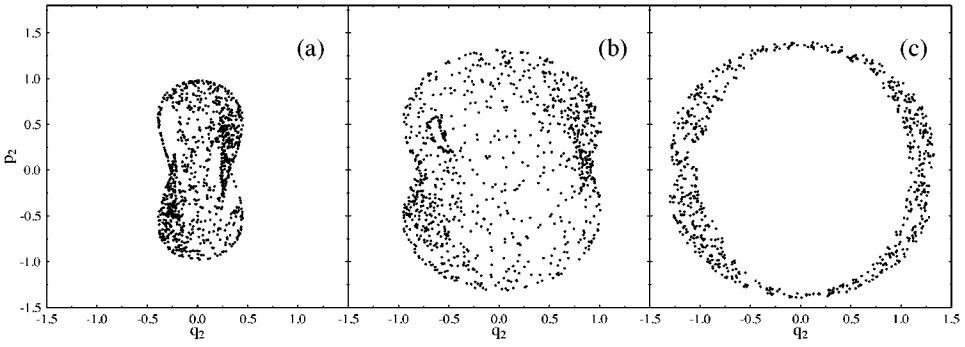

FIG. 4. Same as in Fig. 3 for $\lambda = 2$ and (a) $E = 4$, (b) $E = 43$, and (c) $E = 62$.

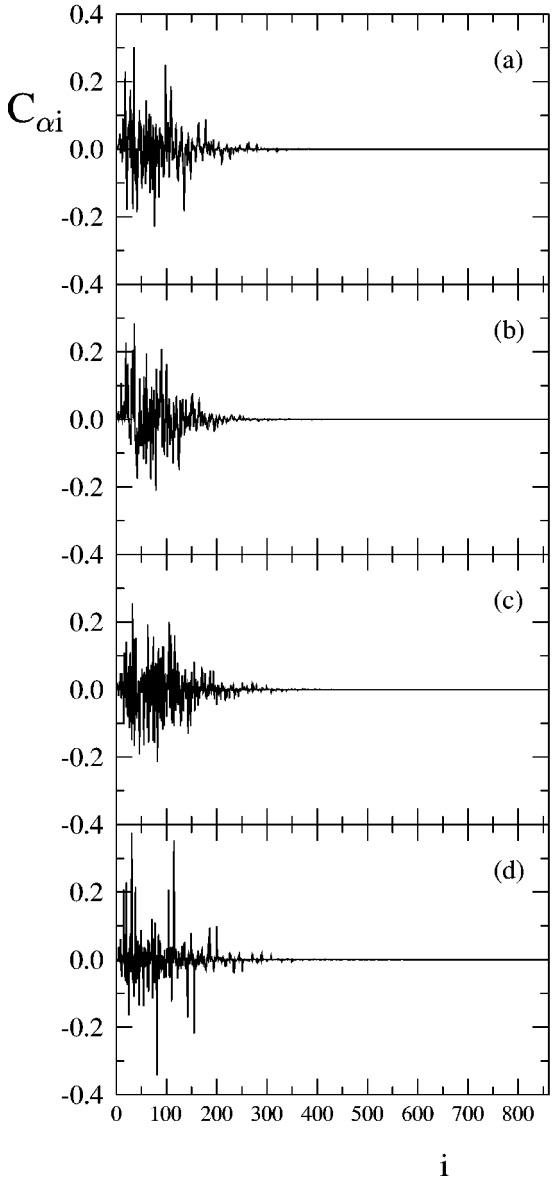

FIG. 5. Four typical eigenstates $|\psi_\alpha\rangle$ of the Hamiltonian H for $\lambda=0.9$ in the basis $|\phi_i\rangle$; (a) $\alpha=50$, (b) $\alpha=51$, (c) $\alpha=52$, (d) $\alpha=53$.

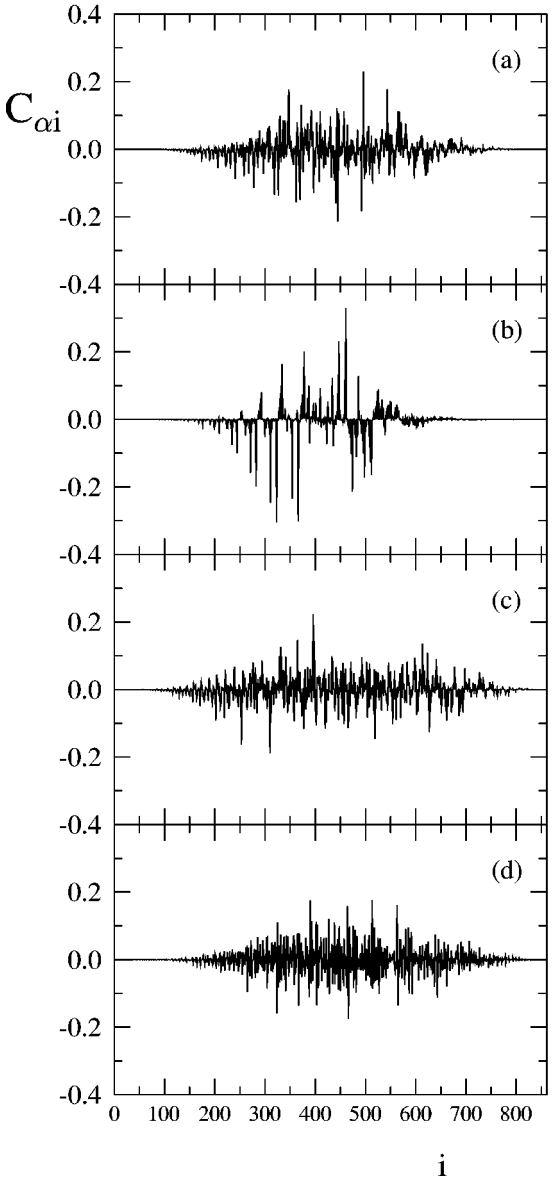

FIG. 6. Same as in Fig. 5 for (a) $\alpha=430$, (b) $\alpha=431$, (c) $\alpha=432$, (d) $\alpha=433$.

matrix elements of $K_{10}K_{10}$ can be regarded as a function of i only. The same is true for the other three operators. The dependence of nonzero matrix elements of the above four operators on i is presented in Fig. 8. Several features can be seen from this figure. First, on average, the nonzero matrix elements of $\mu_1 K_{10}K_{10}$ are relatively large in the low-energy region. Second, apart from the two edges, the average values of the nonzero matrix elements of $\mu_2 K_{20}K_{20}$ are similar in different energy regions. However, in the middle of the energy region, the operator $\mu_2 K_{20}K_{20}$ has many very small nonzero matrix elements. Third, the matrix elements of $\mu_3 K_{21}K_{20}$ are relatively large, on average, in the high-energy region. Finally, the variation of the matrix elements of $\mu_4 K_{12}K_{10}$ in different energy regions is not so large as compared to the other three operators. As a result, the perturbation is stronger in the low- and high-energy regions than in the middle-energy region.

V. STRUCTURE OF LDOS AND EIGENFUNCTIONS

In this section we discuss the shape of the LDOS and of eigenfunctions for the LMG model, we study the classical counterpart of the LDOS, and finally we discuss to what extent the LMG model can be associated with a band random matrix model.

A. Structure of the LDOS and eigenfunctions

The so-called local spectral density of states (LDOS) for an unperturbed state $|\phi_j\rangle$ is defined as

$$w_j(E)=\sum_\alpha |C_{\alpha j}|^2 \delta(E-E_\alpha), \tag{20}$$

where E_α is the eigenenergy of the perturbed eigenstate $|\psi_\alpha\rangle$ and $C_{\alpha j}=\langle\phi_j|\psi_\alpha\rangle$. The function $w_j(E)$, also known as the ''strength function'' or ''Green spectra,'' is quite important

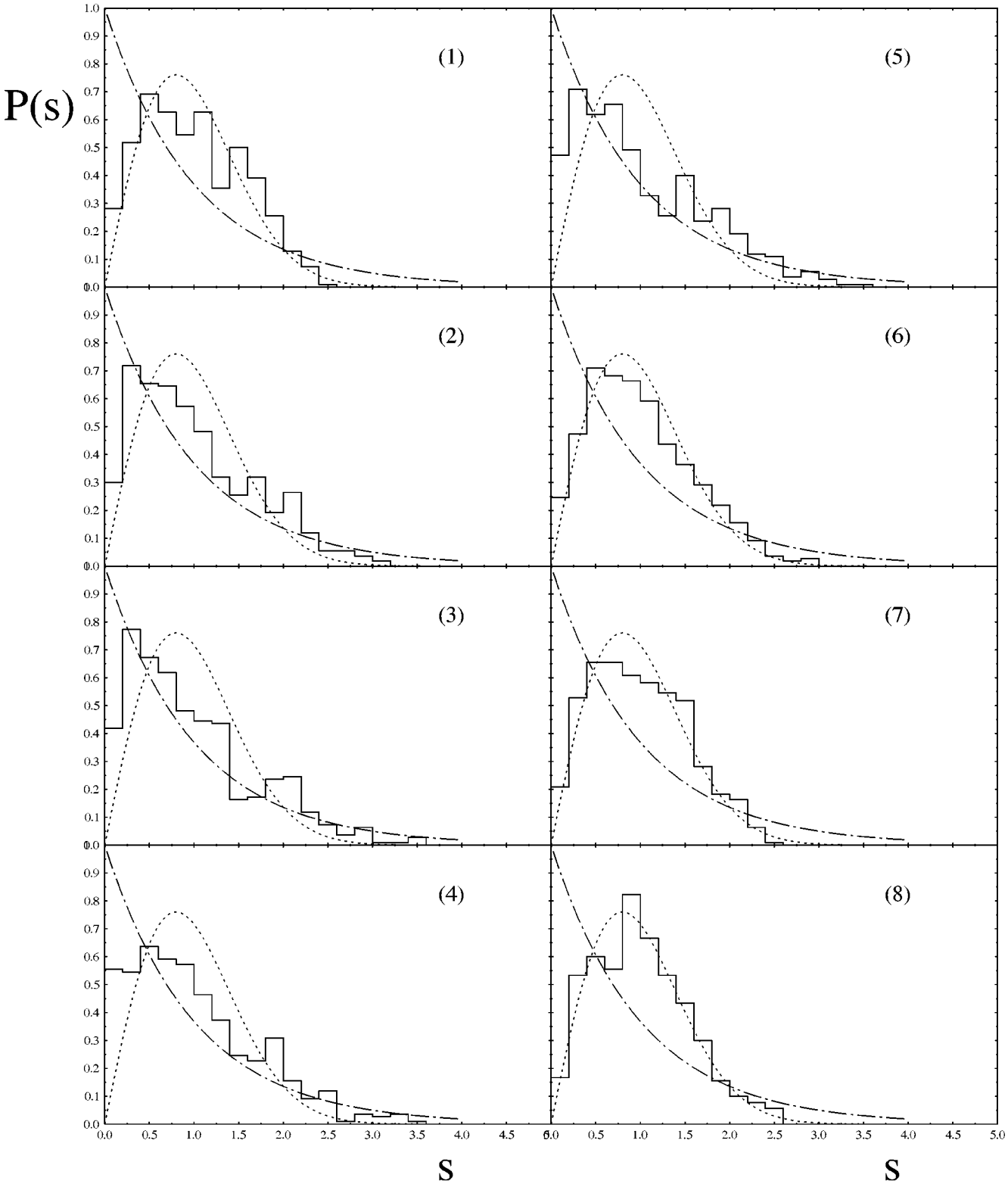

FIG. 7. Histograms of the nearest-level-spacing distributions $P(s)$ for eight energy regions of the Hamiltonian H with $\lambda = 0.9$. (1) $1 < \alpha < 110$, (2) $110 < \alpha < 220$, (3) $220 < \alpha < 330$, (4) $330 < \alpha < 440$, (5) $440 < \alpha < 550$, (6) $550 < \alpha < 660$, (7) $660 < \alpha < 770$, (8) $770 < \alpha < 861$. The dashed and dashed-dotted curves represent the Wigner-Dyson and Poisson distributions, respectively. Each histogram was obtained by diagonalizing five different Hamiltonians with values of λ close to 0.9.

for the understanding of generic properties of the quantum model. In particular, the LDOS shows how the unperturbed state $|\phi_j\rangle$ is coupled to the exact states $|\psi_\alpha\rangle$ with the specific energy E_α. The width of this function (''spreading width'') defines the energy range associated with the ''lifetime'' of an unperturbed state $|\phi_j\rangle$.

The form of the LDOS for band random matrices has been analytically studied by Wigner [14]; see also [3]. Par-

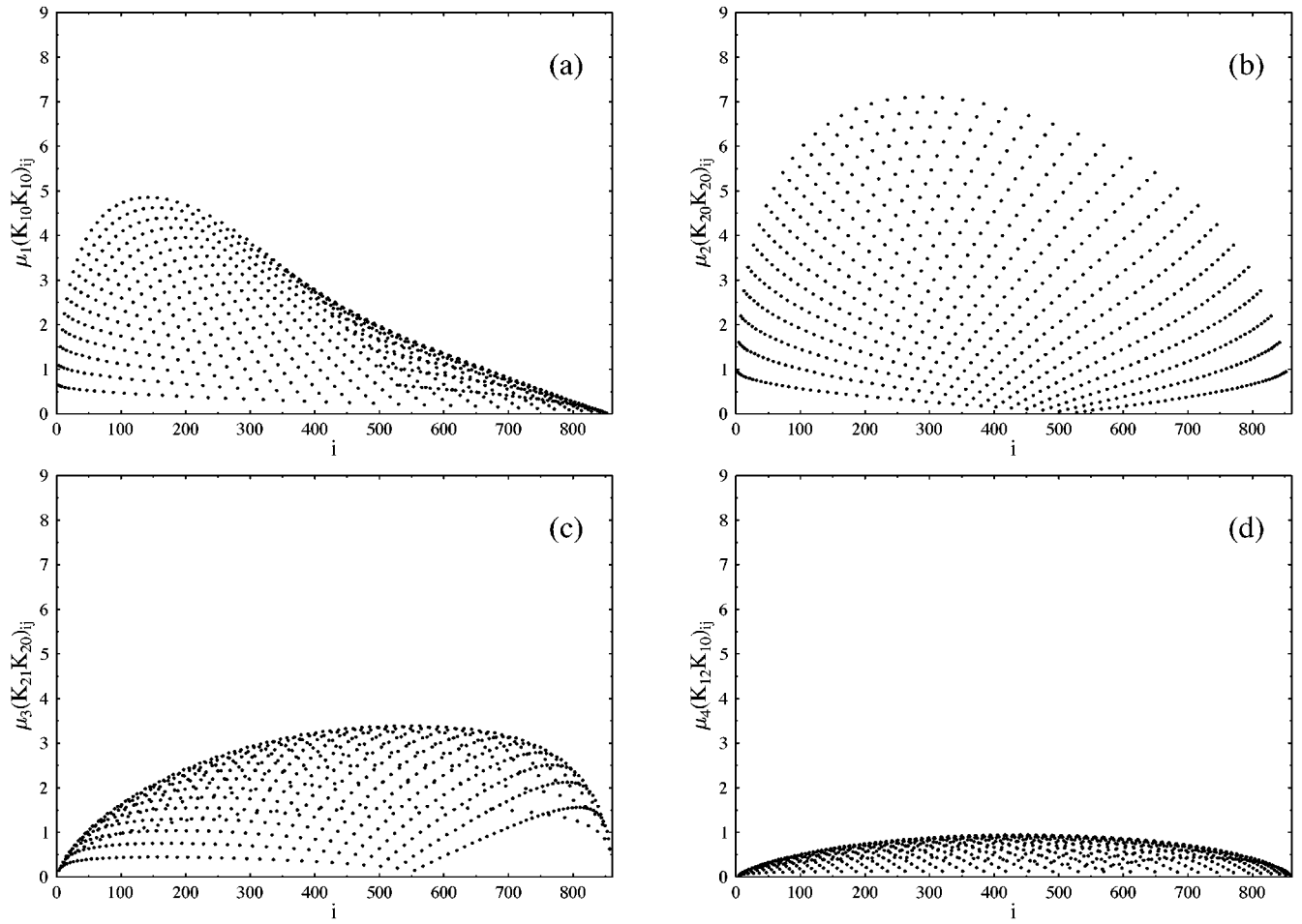

FIG. 8. Nonzero matrix elements of the four operators (a) $\mu_1 K_{10} K_{10}$, (b) $\mu_2 K_{20} K_{20}$, (c) $\mu_3 K_{21} K_{20}$, and (d) $\mu_4 K_{12} K_{10}$. Each operator couples a basis state $|\phi_i\rangle$ to at most only one other basis state $|\phi_j\rangle$.

ticularly, it was shown that when perturbation is not large the LDOS has the form

$$w_{BW}(E-E_j^0)=\frac{\Gamma/2\pi}{(E-E_j^0)^2+\Gamma^2/4}, \tag{21}$$

which is nowadays known as the Breit-Wigner (BW) law. Here, Γ is the half-width of the distribution. For larger perturbations, the form of the LDOS becomes model dependent and in the intermediate region can be approximately described by a Gaussian distribution [26].

Another important quantity is the shape of eigenfunctions (EFs)

$$W_\alpha(E^0)=\sum_j |C_{\alpha j}|^2 \delta(E^0-E_j^0) \tag{22}$$

in the unperturbed energy basis. In our numerical calculations of the LDOS and EFs for the LMG model, in order to suppress fluctuations, we have taken averages over 200 of individual distributions in the interval $331 \leqslant j \leqslant 530$ for the LDOS and $331 \leqslant \alpha \leqslant 530$ for the EFs. The averaged distributions will be denoted by $w(E)$ and $W(E^0)$, respectively. Before averaging, we should first express $w_j(E)$ and $W_\alpha(E^0)$ with respect to their centroids, respectively. For the LDOS, the centroid of $w_j(E)$ is just E_j^0 [2],

$$E_j^0=\sum_\alpha E_\alpha |C_{\alpha j}|^2, \tag{23}$$

so that we can express the LDOS as $w_j(E-E_j^0)$. On the other hand, the centroid of $W_\alpha(E^0)$, labeled by e_α, is defined by

$$e_\alpha=\sum_j E_j^0 |C_{\alpha j}|^2, \tag{24}$$

and W_α can be expressed as a function of the shift (E^0-e_α).

The dependence of the shape of the LDOS and EFs on the perturbation is presented in Fig. 9. The left column gives the LDOS and the right column shows the EFs. (Notice that the vertical scale depends on the value of λ.). The first remark is that the shapes of the LDOS and of the EFs are quite similar when the perturbation is not large ($\lambda \leqslant 0.9$). On the other hand, with increasing λ, they start to deviate from each other. Another result is that for not large perturbation, $\lambda \leqslant 0.9$, there seem to be large peaks that are not washed out by the averaging process over 200 distributions. In fact, they come from dynamical interference (correlation) effects, which will be explained in Appendix B.

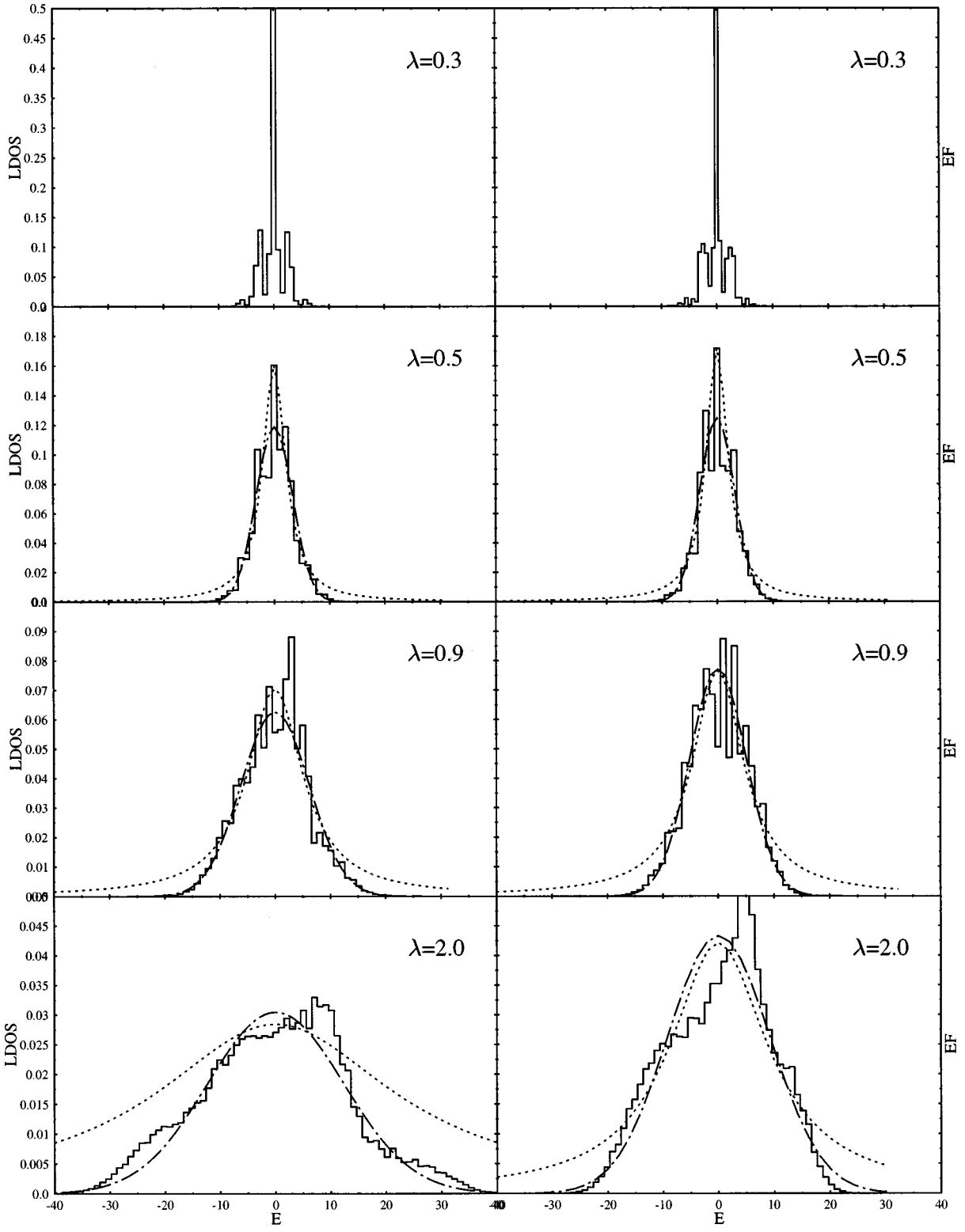

FIG. 9. Averaged LDOSs (left column histograms) and eigenfunctions (EF) (right column histograms) for the LMG model with different values of λ. Dashed and dashed-dotted curves are fitting curves to the BW and Gaussian forms, respectively.

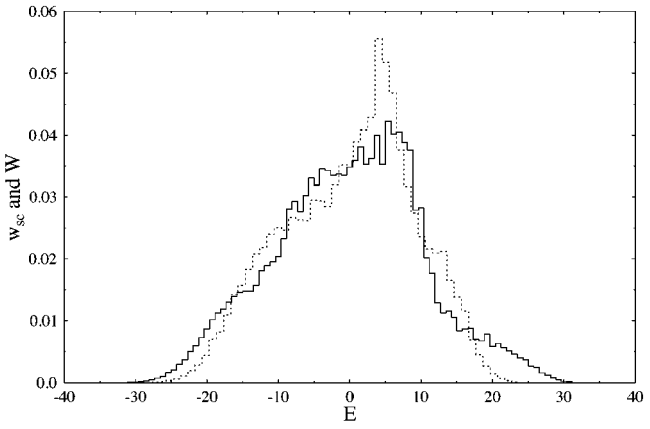

FIG. 10. A comparison between the rescaled LDOS $w_{sc}(E)$ (solid histogram) and the EF $W(E^0)$ for $\lambda=2$ (dashed histogram).

The dashed curves in Fig. 9 correspond to the best fit to the BW form and the dashed-dotted curves correspond to the best fit to the Gaussian form. The fitting was made here for the central parts of the LDOS and EFs. Specifically, neglecting the long tails, we chose for the fitting only the data with w and W larger than 0.01.

In Fig. 9 it can be seen that for $\lambda=0.5$ the central parts of both distributions can be well fitted by both the BW and Gaussian forms (however, the agreement with the Gaussian form extends to the region of the tails). For stronger perturbation $\lambda=0.9$, the distributions can still be fitted quite well by the Gaussian form. Finally, when the perturbation is very strong, for example, $\lambda=2.0$ the LDOS and EFs deviate, as expected, from both the BW and the Gaussian forms.

The difference between the LDOS and the EFs for large perturbations $\lambda=2.0$ is quite evident; however, one should note that the LDOS is plotted in the perturbed energy basis, while the EF is plotted in the unperturbed one. Therefore, in order to make the comparison meaningful, one should rescale the distribution in a proper way. We use the same rescaling as in Fig. 2(c). After this rescaling (see Fig. 10) they look more similar to each other than in Fig. 9.

B. The classical limit of LDOS

The classical counterpart of the LDOS, in short, the classical LDOS, labeled by $w_{cl}(E-E_j^0)$, can be defined as the probability that a phase point, which belongs to the torus corresponding to the quantum numbers m_j and n_j of $|\phi_j\rangle$, has total energy E [4]. It is expressed as a function of the distance $(E-E_j^0)$ where E_j^0 is the unperturbed energy of the torus m_j, n_j. According to Eq. (15), in the limit $\Omega\to\infty$, we have

$$\frac{b_r^\dagger b_r}{\Omega}=\frac{(p_r^2+q_r^2)}{2}. \tag{25}$$

Thus, the torus corresponding to m_j and n_j is that with $(p_1^2+q_1^2)=2m_j/\Omega$ and $(p_2^2+q_2^2)=2n_j/\Omega$.

In analogy to the quantum case, the classical LDOS was averaged over 200 different tori. In Fig. 11, we show a comparison between the quantum and classical LDOS for $\lambda=0.3, 0.5, 0.9$, and 2.0. As discussed in Appendix B, the LDOS for $\lambda=0.3$ depends on strong dynamical quantum correlations; as is seen from the figure, in the classical limit these correlations disappear. At the same time, the shape of the classical LDOS is, on average, close to the quantum one, apart from the tails, which are of quantum origin and are due to tunneling effects. The data also show that, by increasing the perturbation, the agreement becomes better. The main difference for $\lambda=2.0$ is that in the center the LDOS is lower than the classical LDOS. This may be related to a result given in Ref. [3] that there is a local minimum in the center of the LDOS for relatively strong perturbations.

C. A band random matrix model

Recently it has been shown that realistic conservative systems with chaotic properties can be approximated by band random matrices [1,7–9]. Therefore, it is very interesting to check whether the Hamiltonian of the LMG model, which does not contain any random matrix element, see Eq. (10), can be associated with an ensemble of random matrices. To be as close as possible to the dynamical model, we introduce here band random matrices of the form

$$H_{ran}=H_0+\lambda V_{ran}, \tag{26}$$

where H_0 is the same as for the LMG model, see Eq. (5), and V_{ran} is obtained by replacing the nonzero matrix elements of V of the LMG model by random numbers with Gaussian distribution. The mean value of the matrix elements $(V_{ran})_{kl}$ is zero and the variance, averaged over the nonzero matrix elements, is taken to be the same as in the dynamical LMG model $\langle (V_{ran})_{kl}^2\rangle=\langle V_{kl}^2\rangle$.

Numerical data for both the LDOS and EFs of H_{ran} are presented in Fig. 12. Averages have also been taken over 200 LDOSs and EFs, respectively, in the central region of the spectrum, as in the calculations of the LMG model. Interestingly, these results are similar to those found for Wigner band random matrices [3]; that is, for small perturbations the central part of the LDOS is of the BW form, while in the transition region when the perturbation is relatively strong, it can be fitted to the Gaussian form; for stronger perturbations it can be fitted approximately to the semicircle law

$$w(E)=\frac{2}{\pi R_0^2}\sqrt{R_0^2-E^2}. \tag{27}$$

From Figs. 12 and 9, it can be seen that the shape of the LDOS and EFs of H_{ran} for $\lambda=0.3, 0.5$, and 0.9 are much smoother than the corresponding LDOS and EFs of the LMG model. This can be explained by the randomness of $(V_{ran})_{kl}$; see Appendix B. Another feature is that the central parts of the LDOS and of the EFs for $\lambda=0.3$–0.9 in Fig. 12 are lower than those for the LMG model. This also is an effect of interference. Finally, comparing the two figures, it can be seen that for $\lambda\leqslant 0.9$ the central parts of LDOS and EFs of the LMG model are roughly similar to those of H_{ran}. Thus, when perturbation is not very large, the LMG model can be associated with the above band random matrix model (26).

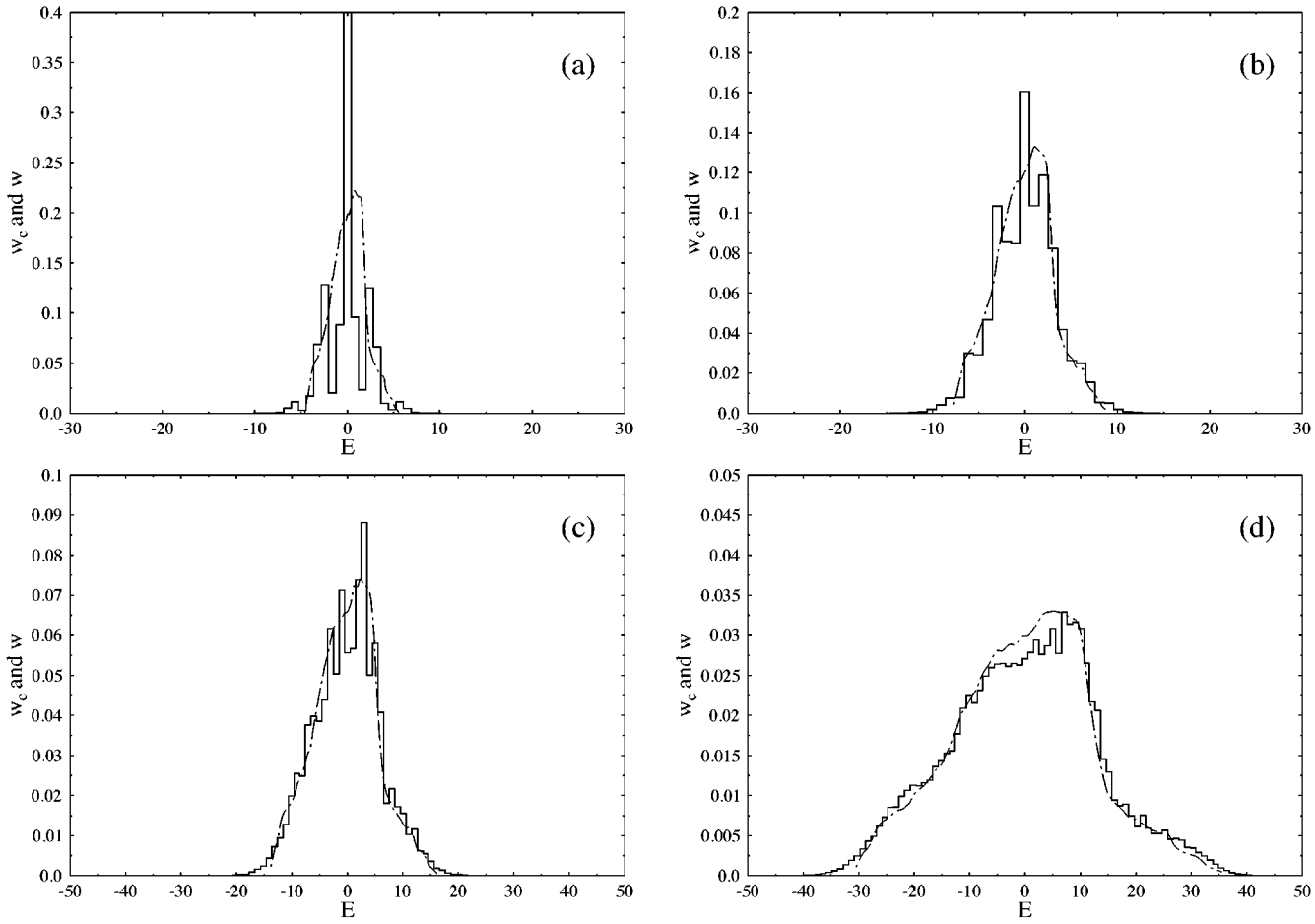

FIG. 11. Classical counterparts of the LDOS (dashed-dotted curves) for (a) $\lambda=0.3$, (b) $\lambda=0.5$, (c) $\lambda=0.9$, and (d) $\lambda=2$. For comparison the corresponding LDOSs are also plotted (solid histograms).

VI. LONG TAILS OF LDOS AND EIGENFUNCTIONS

In the preceding section, we have discussed the central parts of LDOS and EFs. In this section we study their long tails with the help of perturbation theory since, as discussed in Appendix A, long tails are always in the perturbative region.

First we consider the case of small λ for which the coefficients $|C_{\alpha j}|$ decrease very fast as $|E_\alpha - E_j^0|$ increases. Let us start with the left tails of EFs, $E_j^0 << E_\alpha$, with E_α in the middle energy region. From Eq. (A4), we have

$$C_{\alpha j}^2 \equiv |\langle \phi_j | \psi_\alpha \rangle|^2 = \left| \frac{\langle \phi_j | \lambda V | \psi_\alpha \rangle}{E_\alpha - E_j^0} \right|^2 . \tag{28}$$

As indicated in Sec. II, there are only eight basis states that can be coupled with a given basis state $|\phi_j\rangle$ by the perturbation V. Denote these states by $|\phi_l\rangle$, $l=l_1,l_2,\ldots,l_8$ in order of increasing energy. Notice that since the energy differences $d^{(t)}$ are generally much larger than the local level spacings [about 0.1, on average; see Fig. 2(a)], there are many basis states located between each two of the above eight states $|\phi_l\rangle$. Therefore, if the term $|C_{\alpha k}|^2$ decreases fast enough with decreasing k in the region $E_k^0 \ll E_\alpha$, the component $|C_{\alpha k}|$ for $k=l_8$ will be much larger than the sum of the other seven components; then,

$$C_{\alpha j}^2 \approx \frac{(\lambda V_{jl8}^{(2)})^2}{(E_\alpha - E_j^0)^2} C_{\alpha l8}^2 . \tag{29}$$

Following the procedure given in Appendix D of Ref. [1], one obtains the following estimate for the left tails of the averaged EFs:

$$W(\xi) \propto \exp\left\{ -2\xi \ln\left(\frac{\xi}{e} \frac{2\epsilon_2}{\lambda v^{(2)}} \right) \right\} \tag{30}$$

where $\xi = |E_\alpha - E_j^0|/2\epsilon_2$ and $v^{(2)}$ is the average strength of $V^{(2)}$ in the low-energy region [$V_{jl8}^{(2)}$ in Eq. (29) is in the low-energy region].

For the right tails of EFs, $E_j^0 \gg E_\alpha$, similar arguments lead again to Eq. (30), with $v^{(2)}$ changed to the average strength of $V^{(2)}$ in the high-energy region, which, according to Fig. 8, is approximately equal to the one in the low-energy region.

To obtain an expression for the tails of LDOSs for $|\phi_j\rangle$ with E_j^0 in the middle energy region, we assume that in the regions of tails the shapes of different eigenstates are similar, on average; that is,

$$\overline{C_{\alpha l8}^2} \approx \overline{C_{\alpha' j}^2} \tag{31}$$

for $E_{\alpha'} - E_j^0 \approx E_\alpha - E_{l8}^0$. Then Eq. (29) gives

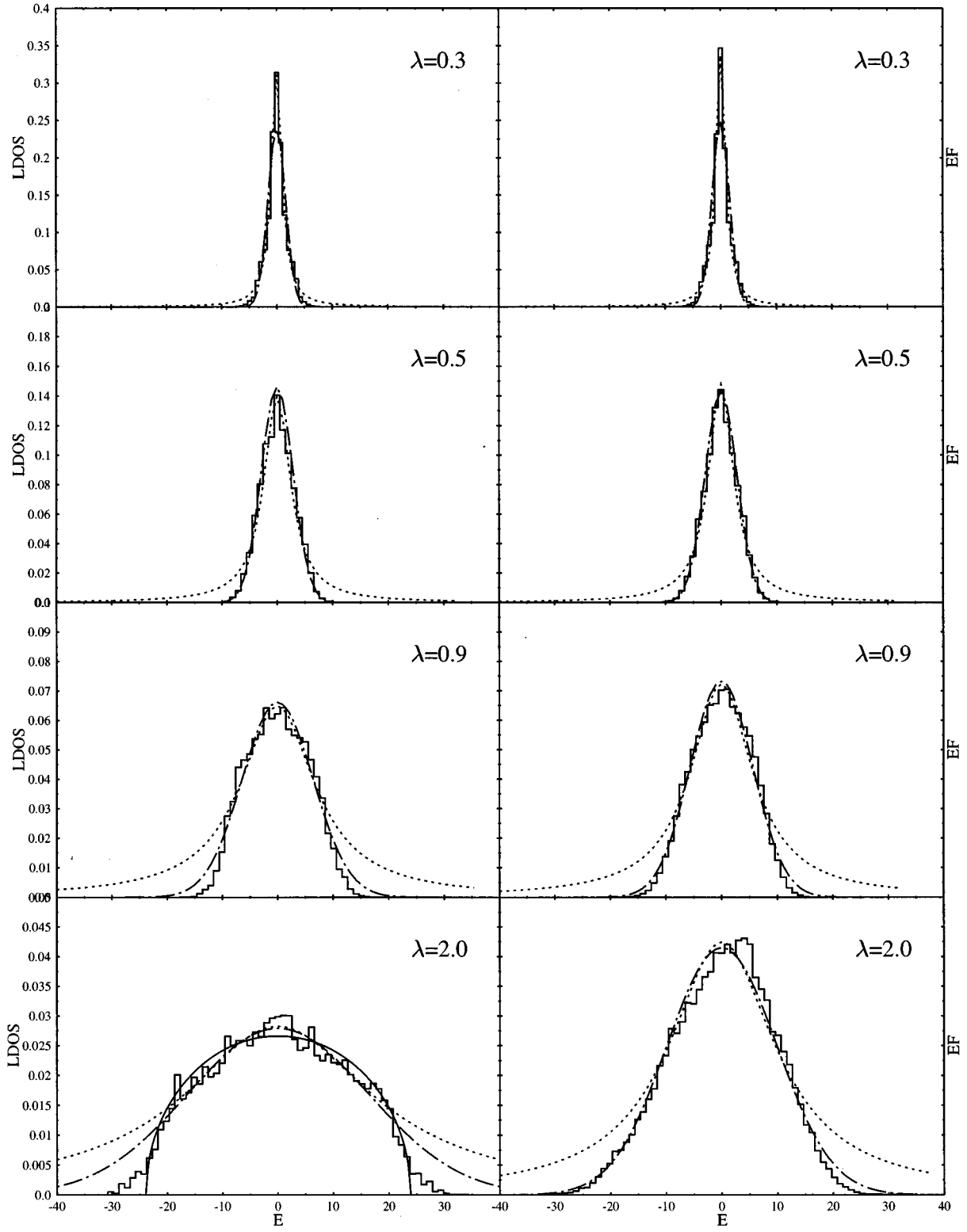

FIG. 12. Same as in Fig. 9 but for the band random matrix model H_{ran}. The solid curve for the LDOS at $\lambda = 2.0$ is the fitting curve to the semicircle law, Eq. (27), with $R_0 \approx 23.9$.

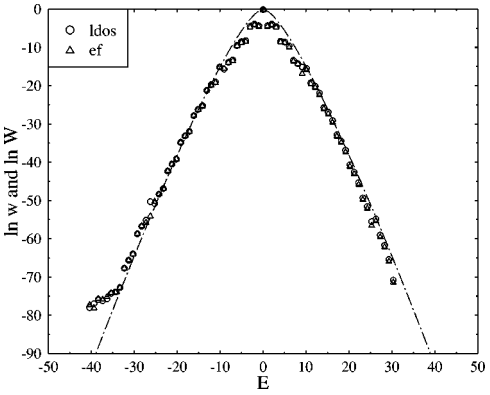

FIG. 13. Numerically computed LDOSs (circles) and EFs (triangles) for $\lambda=0.1$. Each value represents an average over 200 states. The dashed-dotted curve gives the analytical prediction (30) (with the appropriate normalization factor) for the long tails.

$$C_{\alpha j}^2 \approx \frac{(\lambda V_{j18}^{(2)})^2}{(E_\alpha - E_j^0)^2} C_{\alpha' j}^2, \tag{32}$$

and, for the two tails of the LDOS, one obtains the same expression as Eq. (30), with $\xi=|E_\alpha-E_j^0|/2\epsilon_2$ and $v^{(2)}$ the average strength of $V^{(2)}$ in the middle energy region [$V_{j18}^{(2)}$ in Eq. (32) is in the middle-energy region].

When λ is not small, as indicated in Appendix B, more research work is needed in order to obtain an analytical expression for the tails of EFs and LDOSs. However, we can assume that the tails obey a law somewhat similar to Eq. (30), with $v^{(2)}$ changed to v (since when λ is not small, the tails are determined not only by $V^{(2)}$, but also by the other $V^{(t)}$). Here, similar to the small λ case, v is the average strength of the perturbation in the corresponding regions: for the left and right tails of EFs, the average should be taken in the low- and high-energy regions, respectively, while for the two tails of the LDOS the average should be taken in the middle-energy region. According to Fig. 8, the value of v in the low-energy region is larger than that in the high-energy region, so the right tail of the EF should drop faster than the left one, while the two tails of the LDOS should be similar.

We have numerically computed the tails of both the LDOS and EFs for the case of weak perturbation $\lambda=0.1$, and the results are shown in Fig. 13 in logarithm scale. Each point represents an average over 200 states. It can be seen that the tails of LDOSs and EFs are quite close to each other, in agreement with the fact that, for small λ, they obey the same law given by Eq. (30) with similar values of $v^{(2)}$. Also the agreement between the numerical results and the analytical prediction is quite good.

When the perturbation increases to $\lambda=0.3$, the tails begin to deviate from the prediction (30). However, it has been found that for $\lambda\geq 0.3$ the tails can be fitted quite well to the expression (30), with v instead of $v^{(2)}$ and ξ given by

$$\xi=\left(\frac{|E_\alpha-E_j^0|-x_0}{10\epsilon_2}\right)^2, \tag{33}$$

where x_0 is an adjusting parameter. As an example we present in Fig. 14 the results for $\lambda=0.9$. The LDOS and its fitting curve with $x_0=13$ are given in Fig. 14(a). It can be seen that the agreement is quite good, not only in the long tail regions, but also in the regions quite close to the central part. Figure 14(b) gives the tails for the EF and the fitting curve with $x_0=16$. The figure also verifies the prediction given above that the right tail drops faster than the left one for the EF, while the two tails are similar for the LDOS.

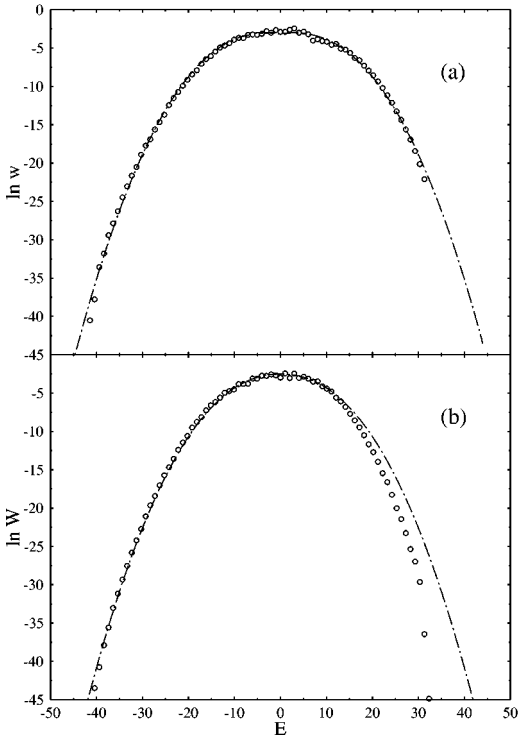

FIG. 14. (a) LDOS (circles) for $\lambda=0.9$ and the fitting curve (dashed-dotted curve) given by Eqs. (30) and (33) with $x_0=-13$. (b) Similar to (a) for the EF (circles) with $x_0=-16$.

For the band random matrix model (26), as indicated in Appendix B, the long tails of EFs and LDOSs obey the same law given by Eq. (30). This has been confirmed by numerical results. As an example, in Fig. 15 we present the tails of LDOS for $\lambda=0.9$ and the prediction given by Eq. (30). The agreement between numerical data and the analytical result is again quite good in the long tail regions.

VII. CONCLUSIONS AND DISCUSSION

In this paper we have studied the Lipkin-Meshkov-Glick (LMG) model in the many-particle basis of noninteracting

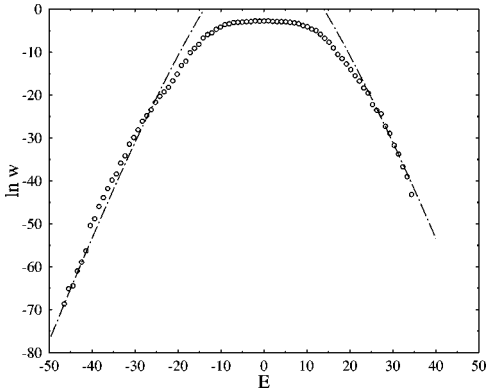

FIG. 15. LDOS (circles) of H_{ran} in Eq. (26) for $\lambda=0.9$ and the theoretical prediction (30) (dashed-dotted curve) for its long tails.

particles. Main attention has been paid to the structure of the local spectral density of states (LDOS) in comparison with that of eigenfunctions (EFs) defined in the unperturbed energy basis.

Due to its dynamical nature, the properties of the LMG model strongly depend on the energy region. Namely, for strong enough perturbation λ, chaotic properties of the model for low and high excitation energies are stronger than in the middle of the energy spectrum. This fact is explained both on the grounds of peculiarities of the quantum model and of its classical counterpart. In particular, the eigenstates in the middle of the spectrum are more regular, as compared with the eigenstates for low and high energies; correspondingly, the level spacing distribution is close to the Wigner-Dyson type at the edges of the spectrum, unlike in the center of the spectrum where deviations from the Wigner-Dyson form have been detected.

One of the main questions addressed in our study is the dependence of the shape of LDOSs and EFs on the perturbation strength. Numerical analysis has shown that for relatively weak perturbations the form of the LDOS is close to the Breit-Wigner form, apart from the tails. This fact is in accordance with several observations for models with random interaction described by different random matrix ensembles [1,3]. However, detailed studies of LDOSs and EFs for the LMG model in the region of not very strong interaction have revealed remarkable correlations that can be analytically explained. In fact, these correlations are due to the dynamical nature of the model, and they are found to be washed out for stronger interaction.

With the increase of perturbation, the form of the LDOS changes, and for a quite moderate perturbation it is well described by a Gaussian distribution. This observation is quite interesting in view of recent numerical data for complex atoms [1] and heavy nuclei [2], where the form of the LDOS was found to be quite close to a Gaussian one. The same effect (the change of the form of LDOSs from Breit-Wigner to Gaussian-like) has also been found in numerical investigations of Wigner band random matrices [26]. Therefore, our data for the dynamical LMG model indicate that the above fact is of a quite generic nature and occurs also in dynamical models exhibiting strong chaos in the classical limit. Finally, when the perturbation is very strong, the LDOS has been found to have a quite specific form that is related to the peculiarity of the model under consideration.

Another problem is the relation between the shape of the LDOS and that of EFs. We have found that after a proper rescaling, the shape of the EFs is similar to the shape of the LDOS, if the perturbation is not very strong. This result indicates the absence of localization in the energy shell, which has been found in Wigner band random matrices [4].

As was noticed in [4], the shapes of both LDOSs and EFs have an analogy in the classical limit. In our paper the relation between the LDOS and the corresponding classical quantity has been checked in a dynamical model with a chaotic classical counterpart (see also the recent paper [27]). Numerical analysis of the classical model has shown that the form of the LDOS is close to its classical counterpart if the perturbation is not very weak. This fact allows us to expect that (in semiclassical regions) the global structure of both the LDOS and EFs can be directly found from the corresponding classical model. This is important in view of recent results [19,22] revealing the direct connection of the shape of EFs to the partition function of isolated systems.

Of special interest is the question about the applicability of random matrix models to a given dynamical system in a chaotic region. There are many examples when full random matrices or band random matrices can serve as good models for the description of statistical properties of spectra and eigenstates of dynamical models. However, in these examples the two-body nature of an interaction is, typically, not taken into account. In this paper we have carefully analyzed the possibility of a random matrix description of the model in the energy region where the corresponding classical system can be treated as a chaotic one. Specifically, we have used the same unperturbed part of the Hamiltonian, but with off-diagonal matrix elements chosen at random with the same variance as in the original dynamical model, keeping zero matrix elements that are due to the specific form of the interaction. This approach also allows us to reveal to what extent the underlying correlations of the dynamical model are essential for its statistical description. Numerical results with such a random model have shown a quite good agreement for global properties of the LDOS and chaotic EFs. In particular, the shapes of LDOSs and EFs turn out to remain similar in a large range of the perturbation strength. On the other hand, the form of the LDOS and EFs in the random model turns out to be smoother and does not reveal any regular deviations due to quantum-dynamical correlations, which, for a weak interaction, are significant in the dynamical model.

Finally, the question of the long tails of LDOS and EFs has been studied in detail, both analytically and numerically. For this, a generalized approach has been developed based on the standard Brillouin-Wigner perturbation expansion. Namely, the perturbation theory has been extended to strong perturbation in the region of long tails. This has allowed us to find the analytical form for the long tails of the LDOS and EFs. Numerical data have shown a good agreement with the analytical predictions.

ACKNOWLEDGMENTS

The authors are grateful to I. Guarneri for valuable discussions. W.-G.W. and F.M.I. wish to thank their colleagues of the University of Milano at Como for their hospitality during the period when this work was done. F.M.I. acknowledges the support received from the Cariplo Foundation for Scientific Research as well as the partial support from Grant No. INTAS-94-2058. Partial support of the National Basic Research Project ''Nonlinear Science,'' China, the Natural Science Foundation of China, and the Post-doctoral Foundation of China is also gratefully acknowledged by W.-G.W.

APPENDIX A: BRILLOUIN-WIGNER PERTURBATION EXPANSION OF EIGENSTATES

Here we introduce a generalization of the so-called Brillouin-Wigner perturbation expansion [28,29], which can be shown to be valid even for strong perturbations. In particular, we show that long tails are always in the perturbative region, and this also explains some previous results [1,3,4].

First, we divide the set of basis vectors, i.e., the eigenstates of H^0, into two parts, $\{|\phi_i\rangle, i=p_1,\ldots,p_2\}$ and $\{|\phi_i\rangle, i=1,\ldots,p_1-1,p_2+1,\ldots,N\}$. Correspondingly, there are two projection operators

$$P=\sum_{i=p_1}^{p_2}|\phi_i\rangle\langle\phi_i|, \quad Q=1-P. \tag{A1}$$

The subspaces related to P and Q will be called, in the following, the P and Q subspaces, respectively. We now split an arbitrary eigenstate $|\psi_\alpha\rangle$ of H into two orthogonal parts

$$|\psi_\alpha\rangle=|t\rangle+|f\rangle, \quad \langle t|f\rangle=0, \tag{A2}$$

where $|t\rangle=P|\psi_\alpha\rangle$ and $|f\rangle=Q|\psi_\alpha\rangle$. Applying Q to the Schrödinger equation (13), we readily obtain

$$[E_\alpha-H^0]|f\rangle=Q\lambda V|\psi_\alpha\rangle; \tag{A3}$$

then,

$$|\psi_\alpha\rangle=|t\rangle+\frac{1}{E_\alpha-H^0}Q\lambda V|\psi_\alpha\rangle, \tag{A4}$$

in which the eigenstate $|\psi_\alpha\rangle$ can either be normalized or not. We remark that in the particular case in which $|t\rangle$ is chosen as a single basis state $|\phi_i\rangle$ $(i=\alpha)$ and E_α taken as

$$E_\alpha=E_i^0+\langle\phi_i|\lambda V|\psi_\alpha\rangle, \tag{A5}$$

then the iterative expansion of Eq. (A4) is just the Brillouin-Wigner perturbation expansion, in which the eigenstate $|\psi_\alpha\rangle$ is not normalized.

Since our purpose is to study the structure of eigenfunctions and of the LDOS, and not to solve the eigenvalue problem, we take E_α in Eq. (A4) as a constant, i.e., its exact (unknown) value, which can be find out by other methods. Then the iterative expansion of Eq. (A4) gives

$$\begin{aligned}|\psi_\alpha\rangle=&|t\rangle+\frac{1}{E_\alpha-H^0}Q\lambda V|t\rangle\\&+\frac{1}{E_\alpha-H^0}Q\lambda V\frac{1}{E_\alpha-H^0}Q\lambda V|t\rangle+\cdots\\&+\left(\frac{1}{E_\alpha-H^0}Q\lambda V\right)^{n-1}|t\rangle+\left(\frac{1}{E_\alpha-H^0}Q\lambda V\right)^{n}|\psi_\alpha\rangle.\end{aligned} \tag{A6}$$

If the last term on the right-hand side of Eq. (A6), denoted by T_n, tends to zero when $n\to\infty$, one has a *generalization of Brillouin-Wigner perturbation expansion* (GBWPE), which gives an exact expression for $|\psi_\alpha\rangle$ in terms of $|t\rangle$, E_α, λV, and H^0:

$$\begin{aligned}|\psi_\alpha\rangle=&|t\rangle+\frac{1}{E_\alpha-H^0}Q\lambda V|t\rangle+\left(\frac{1}{E_\alpha-H^0}Q\lambda V\right)^{2}|t\rangle+\cdots\\&+\left(\frac{1}{E_\alpha-H^0}Q\lambda V\right)^{q}|t\rangle+\cdots.\end{aligned} \tag{A7}$$

For example, for a Hamiltonian matrix with band structure and perturbation V coupling a basis state to at most b other states, if the Q subspace is chosen, such that for $|\phi_j\rangle$ in the Q subspaces $|E_\alpha-E_j^0|\geqslant bV_{max}$, where V_{max} is the maximum of the absolute value of (λV_{ij}), then T_n will approach zero when n goes to infinity.

For each state $|\psi_\alpha\rangle$, there exists a P subspace with the minimum number of basis states (denoted by P_{min}) and correspondingly a Q subspace with the maximal number of basis states (denoted by Q_{max}) that ensure that Eq. (A7) holds. Clearly, from Eq. (A7), the components of the state $|\psi_\alpha\rangle$ in the Q subspace are in the perturbative region. Therefore, the expansion of the exact state $|\psi_\alpha\rangle$ in the basis $|\phi_j\rangle$ is naturally divided into two parts: the nonperturbative part $|t_{min}\rangle\equiv P_{min}|\psi_\alpha\rangle$ and the perturbative part $|f_{max}\rangle\equiv Q_{max}|\psi_\alpha\rangle$. Tails of $|\psi_\alpha\rangle$ are always in the perturbative region and can be studied with the GBWPE. The same approach can be applied to the LDOS, which can also be divided into two parts, perturbative and nonperturbative.

APPENDIX B: A ''PATH'' APPROACH TO PERTURBATIVE EXPANSION

In order to study the perturbative part of $|\psi_\alpha\rangle$ in the GBWPE given in Eq. (A7), we make use of the concept of path, in analogy to that in the Feynman's path integral theory [30]. First we discuss the case of small perturbations. In this case, the term $|t\rangle$ can be chosen as the basis state $|\phi_i\rangle$ with the smallest value of $|E_\alpha-E_i^0|$. For an arbitrary $|\phi_j\rangle$ in the Q subspace, Eq. (A7) gives

$$\begin{aligned}C_{\alpha j}\equiv\langle\phi_j|\psi_\alpha\rangle=&\frac{\lambda V_{ji}}{E_\alpha-E_j^0}+\sum_{k\in Q}\frac{\lambda V_{jk}}{E_\alpha-E_j^0}\frac{\lambda V_{ki}}{E_\alpha-E_k^0}\\&+\sum_{k,l\in Q}\frac{\lambda V_{jk}}{E_\alpha-E_j^0}\frac{\lambda V_{kl}}{E_\alpha-E_k^0}\frac{\lambda V_{li}}{E_\alpha-E_l^0}\cdots.\end{aligned} \tag{B1}$$

We now term a sequence $j\to k_1\to\cdots\to k_{q-1}\to i$ a path of q paces from j to i, if the matrix elements of the perturbation $V_{kk'}$ corresponding to each pace are nonzero. Attributing a factor $\lambda V_{kk'}/(E_\alpha-E_k^0)$ to each pace $k\to k'$, the contribution of a path to $C_{\alpha j}$ is the product of the factors of all its paces. Then, the qth term of $C_{\alpha j}$ on the right-hand side of Eq. (B1) can be rewritten as

$$F_q(j\to i)=\sum_s f_{q,s}(j\to i), \tag{B2}$$

where s indicates the paths with q paces from j to i and $f_{q,s}(j\to i)$ is the contribution of the path s to $C_{\alpha j}$. Defining $A(j\to i)$ as

$$A(j\to i)=\sum_{q=q_0}^{\infty}F_q(j\to i), \tag{B3}$$

where q_0 is the number of the paces of the shortest path from j to i, we have

$$C_{\alpha j}=A(j\to i) \tag{B4}$$

for small λV.

For the general case, the term $|t\rangle$ cannot be chosen as a single basis vector, but must be a superposition of some basis vectors. Writing

$$|t\rangle=\sum_{i=p_1}^{p_2} t_i|\phi_i\rangle, \tag{B5}$$

$C_{\alpha j}=\langle\phi_j|\psi_\alpha\rangle$ can be expressed as

$$C_{\alpha j}=\sum_{i=p_1}^{p_2} A(j\rightarrow i)t_i. \tag{B6}$$

For Hamiltonians with band structure, paths have qualitatively different features for small and large perturbations. When the perturbation is small, the difference (p_2-p_1), see Eq. (A1), of the P_{min} subspace is smaller than the band width b. A path which start from $j<p_1$, can reach points k larger than p_2, in other words, a path can ''cross'' the P region. Thus, the difference $E_\alpha-E_k^0$ can be both positive and negative. This is important for the parameters we have chosen in Sec. II, which make all the non-zero matrix elements of V positive. When λ is so large that p_2-p_1 is larger than b, paths starting from $j<p_1$ can no longer reach $k>p_2$, i.e., cannot ''cross'' the P region. Hence the values of $E_\alpha-E_k^0$ are either always positive or negative for a path.

The above concept of path is very useful in studying Hamiltonians with band and sparse structures. For the LMG model it is especially useful, since the perturbation V couples a basis state to at most eight others, as shown in Fig. 1. In fact, we have a simple method to find out all possible paths from j to i. First we write the basis vectors $|\phi_i\rangle$ in their equivalent forms $|m_i,n_i\rangle$, with m_i being the number of particles in the orbital 1 and n_i the number of particles in the orbital 2. We denote the changes of m and n along a path by $\Delta m=m_i-m_j$ and $\Delta n=n_i-n_j$, and the changes of m and n for a pace r from $k=k_l$ to $k'=k_{l+1}$ by $\delta m_r=m_{k'}-m_k$ and $\delta n_r=n_{k'}-n_k$. Then, if the path has q paces, we can write

$$\Delta m=\sum_{r=1}^{q}\delta m_r, \quad \Delta n=\sum_{r=1}^{q}\delta n_r. \tag{B7}$$

Since the interchange of r does not influence the sum, Eq. (B7) is also satisfied by some other related paths. According to Eq. (10), there are only eight possible pairs of δm and δn,

$$\begin{aligned}
&\delta m=\pm 2, \quad \delta n=0 \quad \text{for } V^{(1)},\\
&\delta m=0, \quad \delta n=\pm 2 \quad \text{for } V^{(2)},\\
&\delta m=\mp 1, \quad \delta n=\pm 2 \quad \text{for } V^{(3)},\\
&\delta m=\pm 2, \quad \delta n=\mp 1 \quad \text{for } V^{(4)};
\end{aligned} \tag{B8}$$

therefore, in order to find out all possible q-pace paths from j to i, one should just find out all possible combinations of q pairs of the possible δm and δn in Eq. (B8) that satisfy Eq. (B7) (if all the intermediate points are in the Q subspace).

When λ is small, the term $|t\rangle$ in Eq. (A7) can be chosen as one basis vector $|\phi_i\rangle$, and the expanding coefficient $C_{\alpha j}=\langle\phi_j|\psi_\alpha\rangle$ is $A(j\rightarrow i)=\Sigma_q F_q$; see Eq. (B4). As an example, let us consider $C_{\alpha j}$, for which j is determined by $\Delta m=m_i-m_j=2$, $\Delta n=n_i-n_j=0$; i.e., the two unperturbed states $|\phi_i\rangle$ and $|\phi_j\rangle$ are coupled directly by the term $K_{10}K_{10}$ in Eq. (6). Denote the number of the q-pace paths with positive contributions $f_{q,s}$ in F_q [see Eq. (B2)] by N_{q+} and the number of paths with negative $f_{q,s}$ by N_{q-}. For the shortest path with one pace, $N_{1+}=1$, $N_{1-}=0$. There is no path with two paces. For $q=3$, there are 12 paths (e.g., $K_{02}K_{02}\rightarrow K_{20}K_{20}\rightarrow K_{10}K_{10}$), $N_{3+}=11$, $N_{3-}=1$, and for $q=4$, we have $N_{4+}=11$, $N_{4-}=7$. Clearly, the number of short paths with positive $f_{q,s}$ is much larger than that of short paths with negative $f_{q,s}$. Therefore, $|C_{\alpha j}|$ is quite large and the dynamical interference effect is strong. Similarly, for the other seven $|\phi_j\rangle$ that can be coupled directly to $|\phi_i\rangle$ by the other terms of V, $|C_{\alpha j}|$ are also quite large. On the other hand, for $|\phi_j\rangle$, which are not coupled directly to $|\phi_i\rangle$ by V, $|C_{\alpha j}|$ are smaller. In fact, the two peaks beside the main peak in Fig. 9 for $\lambda=0.3$ come from $C_{\alpha j}$ for the eight states $|\phi_j\rangle$ coupled directly by V to the state $|\phi_i\rangle$. For the band random matrix model discussed in Sec. V, since the nonzero matrix elements of V_{ran} have random signs, we have $N_{q+}\approx N_{q-}$, and the dynamical interference effect should be much smaller than that in the LMG model.

Finally, let us offer some discussion about the long tails of LDOSs and EFs when λ is not small. In this case, we should use Eqs. (B3) and (B6). In the region of long tails, for each $A(j\rightarrow i)$ the main contribution comes from the term F_{q_0}. To see this, we give an estimate of $F_q(j\rightarrow i)$. Since one base vector can be coupled to at most eight others by V, the number of possible paths with q paces from j to i is M^q, where $0<M<8$. Then for long tails we have

$$F_q(j\rightarrow i)\approx\left(\frac{Mv}{E_\alpha-\tilde{E}_j^0}\right)^q, \tag{B9}$$

where v is the average coupling strength of the perturbation V, and for large q, $\tilde{E}_j^0$ is approximately equal to E_j^0. When $|E_\alpha-E_j^0|$ is large enough, the value $F_q(j\rightarrow i)$ decreases very fast with increasing q and the main term is the one with the shortest path (q_0 paces) from j to i. Therefore, $C_{\alpha j}$ can be estimated as

$$C_{\alpha j}\approx\sum_i t_i F_{q_0}(j\rightarrow i). \tag{B10}$$

For the LMG model, due to the dynamical interference (correlation) effects, as discussed above, $F_{q_0}(j\rightarrow i)$ for different i may be equally important. In fact, for large q_0, although the number of paces is large, the number of paths is also large and some of the paces at k may have relatively small values of $|E_\alpha-E_k^0|$. Thus it is difficult to obtain an analytical expression for the tails from Eq. (B10).

For the band random matrix model (26), the signs of the nonzero matrix elements of V_{ran} are random. Therefore, as discussed above, dynamical interference effects are not so large as in the LMG model, and the largest term on the right-hand side of Eq. (B10) is the one with the smallest number of paces q_0. Since $d^{(2)}$ is the largest among the four $d^{(t)}$, the shortest path from j to i mainly consists of paces resulting from $V^{(2)}$. Then Eq. (29) also holds and the same expressions for the long tails of EFs and LDOSs as in Eq. (30) can be found.

[1] V. V. Flambaum, A. A. Gribakina, G. F. Gribakin, and M. G. Kozlov, Phys. Rev. A **50**, 267 (1994).
[2] V. Zelevinsky, B. A. Brown, M. Horoi, and N. Frazier, Phys. Rep. **276**, 85 (1996).
[3] Y. V. Fyodorov, O. A. Chubykalo, F. M. Izrailev, and G. Casati, Phys. Rev. Lett. **76**, 1603 (1996).
[4] G. Casati, B. V. Chirikov, I. Guarneri, and F. M. Izrailev, Phys. Lett. A **223**, 430 (1996).
[5] Ph. Jacquod, D. L. Shepelyansky, and O. P. Sushkov, Phys. Rev. Lett. **78**, 923 (1997).
[6] A. D. Mirlin and Y. V. Fyodorov, e-print cond-mat/97002120.
[7] B. V. Chirikov, Phys. Lett. A **108**, 68 (1985).
[8] M. Feingold, D. M. Leitner, and O. Piro, Phys. Rev. A **39**, 6507 (1989).
[9] A. A. Gribakina, V. V. Flambaum, and G. F. Gribakin, Phys. Rev. E **52**, 5667 (1995).
[10] G. Casati, B. V. Chirikov, F. M. Izrailev, and J. Ford, Lect. Notes Phys. **93**, 334 (1979).
[11] F. M. Izrailev, Phys. Rep. **196**, 299 (1990).
[12] Y. V. Fyodorov and A. D. Mirlin, Int. J. Mod. Phys. B **8**, 3795 (1994).
[13] F. M. Izrailev, Chaos Solitons Fractals **5**, 1219 (1995).
[14] E. Wigner, Ann. Math. **62**, 548 (1955); **65**, 203 (1957).
[15] M. Feingold, D. Leitner, and M. Wilkinson, Phys. Rev. Lett. **66**, 986 (1991); J. Phys. A **24**, 1751 (1991).
[16] D. M. Leitner and M. Feingold, J. Phys. A **26**, 7367 (1993).
[17] G. Casati, B. V. Chirikov, I. Guarneri, and F. M. Izrailev, Phys. Rev. E **48**, R1613 (1993).
[18] H. J. Lipkin, N. Meshkov, and A. J. Glick, Nucl. Phys. **62**, 188 (1965).
[19] V. V. Flambaum and F. M. Izrailev, Phys. Rev. E **55**, R13 (1997).
[20] V. V. Flambaum, G. F. Gribakin, and F. M. Izrailev, Phys. Rev. E **53**, 5729 (1996).
[21] V. V. Flambaum, F. M. Izrailev, and G. Casati, Phys. Rev. E **54**, 2136 (1996).
[22] V. V. Flambaum and F. M. Izrailev, Phys. Rev. E **56**, 5144 (1997).
[23] Xu Gong-ou, Gong Jiang-bin, Wang Wen-ge, Yang Ya-tian, and Fu De-ji, Phys. Rev. E **51**, 1770 (1995).
[24] Xu Gong-ou, Wang Shun-jin, and Yang Ya-tian, Phys. Rev. C **36**, 2095 (1987).
[25] D. C. Meredith, S. E. Koonin, and M. R. Zirnbauer, Phys. Rev. A **37**, 3499 (1988).
[26] G. Casati, V. V. Flambaum, and F. M. Izrailev (unpublished).
[27] F. Borgonovi, I. Guarneri, F. M. Izrailev, and G. Casati, e-print chao-dyn/9711005; F. Borgonovi, I. Guarneri, and F. M. Izrailev (unpublished).
[28] J. M. Ziman, *Elements of Advanced Quantum Theory* (Cambridge University Press, Cambridge, 1969), p. 53.
[29] Xu Gong-ou, Wang Wen-ge, and Yang Ya-tian, Phys. Rev. A **45**, 5401 (1992).
[30] R. P. Feynman and R. G. Hibbs, *Quantum Mechanics and Path Integrals* (McGraw-Hill, New York, 1965).